Percolation and Grain Boundary Wetting in Anisotropic Texturally Equilibrated Pore Networks

Soheil Ghanbarzadeh,[1] Maša Prodanović,[1] and Marc A. Hesse[2,3,*]
[1]Department of Petroleum and Geosystems Engineering, The University of Texas at Austin, Austin, Texas 78712, USA
[2]Department of Geological Sciences, The University of Texas at Austin, Austin, Texas 78712, USA
[3]Institute for Computational Engineering and Sciences, The University of Texas at Austin, Austin, Texas 78712, USA
(Received 11 April 2014; revised manuscript received 21 May 2014; published 25 July 2014)

In texturally equilibrated porous media the pore geometry evolves to minimize the energy of the liquid-solid interfaces, while maintaining the dihedral angle θ at solid-solid-liquid contact lines. We present computations of three-dimensional texturally equilibrated pore networks using a level-set method. Our results show that the grain boundaries with the smallest area can be fully wetted by the pore fluid even for $\theta > 0$. This was previously not thought to be possible at textural equilibrium and reconciles the theory with experimental observations. Even small anisotropy in the fabric of the porous medium allows the wetting of these faces at very low porosities, $\phi < 3\%$. Percolation and orientation of the wetted faces relative to the anisotropy of the fabric are controlled by θ. The wetted grain boundaries are perpendicular to the direction of stretching for $\theta > 60°$ and the pores do not percolate for any investigated ϕ. For $\theta < 60°$, in contrast, the grain boundaries parallel to the direction of stretching are wetted and a percolating pore network forms for all ϕ investigated. At low θ even small anisotropy in the fabric induces large anisotropy in the permeability, due to the concentration of liquid on the grain boundaries and faces.

DOI: 10.1103/PhysRevLett.113.048001 PACS numbers: 81.05.Rm, 47.56.+r, 61.43.Gt, 91.60.-x

A porous medium is considered texturally equilibrated if the solid-liquid interface minimizes the surface energy density γ_{sl}. For a system under hydrostatic pressure and with isotropic surface energies, textural equilibrium requires that the mean curvature $\bar{\kappa}$ of the solid-liquid interface is constant [1,2]. This interface divides space into two interpenetrating and nonintersecting subspaces, similar to bicontinuous cubic phases common in biological systems [3,4]. In the porous media considered here, however, the solid phase is polycrystalline and crystallographically distinct grains introduce additional interfaces into the solid subspace [Fig. 1(a)]. These solid-solid interfaces, i.e., the grain boundaries, are considered stationary on the time scale required to reach textural equilibrium, so that the solid-solid surface energy density γ_{ss} is not minimized. The preexisting grain edge network of the polycrystalline solid therefore imposes a structure on the pore space, which is therefore commonly referred to as grain edge porosity [5]. The preexisting grain boundaries also introduce contact lines along which solid-liquid and solid-solid interfaces meet at sharp angles [Fig. 1(b)]. In a thermodynamically stable material at most three interfaces, separating two solid grains and the liquid, can meet at a contact line [6,7]. Mechanical equilibrium at such a contact line requires that $\gamma_{ss} = 2\gamma_{sl}\cos(\theta/2)$, where θ is the dihedral angle. An important property of texturally equilibrated porous media is that the pore network percolates at any porosity for $\theta \leq 60°$ while a percolation threshold exists for $\theta > 60°$ [7].

Textural equilibrium develops if the solid-liquid reaction kinetics are fast or time scales are long and is therefore common in geological systems and partially molten materials. The pore fluid of these systems is often a melt, which is studied after quenching it to a glass. In this case, the pore

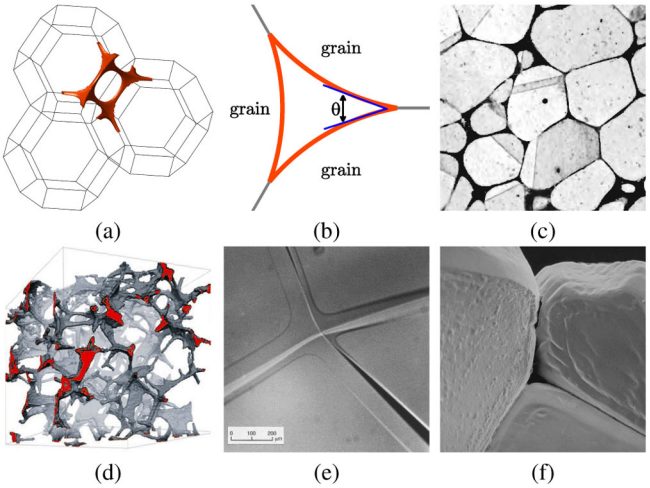

FIG. 1 (color online). (a) Texturally equilibrated pore network with $\theta = 30°$ and $\phi = 1.5\%$ in a polycrystalline solid comprising truncated octahedral grains. (b) Definition of the dihedral angle θ in a cross section of a channel along a three-grain corner. (c) Melt network with $\theta \approx 0°$ in a copper-silver alloy [1]. (d) Melt network with $\phi = 5\%$ in an olivine-basalt aggregate [8] (used with permission from The American Association for the Advancement of Science). (e) Quadruple junction of a melt network between ice grains near 0 °C [9] (used with permission from Nature Publishing Group). (f) Drained brine network in halite with $\theta \approx 45°$ at 1.5 kbar and 395 °C [10] (used with permission from the Geological Society of America).

space is commonly referred to as the intergranular phase and considered part of the microstructure of the material [11]. The percolation of texturally equilibrated intergranular phases was initially studied in the context of two-phase alloys where it controls electrochemical properties [Fig. 1(c)] [1]. In liquid phase sintering textural equilibrium controls the degree of densification [12]. In nuclear engineering the release of fission gases from polycrystalling uranium dioxide is controlled by the formation of texturally equilibrated grain edge porosity [5].

Geological applications include partial melting and melt segregation which control the chemical differentiation of terrestrial planets. Observations suggest both very low porosities yet efficient extraction of partial melt [13–15]. This can be explained by the low θ of melt-rock systems that allows the percolation of texturally equilibrated pore networks at very low porosities [Fig. 1(d)].

Polycrystalline ice also develops a texturally equilibrated water network near its melting point [Fig. 1(e)] [16,17], and even at subzero temperatures in polar ice sheets impurities depress the melting point and give rise to melt networks [18,19]. These water networks provide a fast diffusion path that may displace climate signals recorded in ice cores [9] and provide a habitat for microbial communities [20,21].

The fast reaction kinetics of salt dissolution and precipitation also allow the formation of texturally equilibrated pore networks in rock salt [Fig. 1(f)]. Subsurface salt deposits are generally considered impermeable and hydrocarbon accumulations are often associated with them [22]. The extremely low permeabilities of salt are a consequence of the large salt-brine θ that prevents percolation at low porosities. At the higher pressures and temperatures, however, the salt-brine θ decreases below 60° and allows the formation of a percolating pore network [10,23]. This offers an elegant explanation for field observations of oil impregnated salt [24] and implies that highly radioactive waste stored in rocksalt may come into contact with groundwater if the decay heat increases the temperature sufficiently to allow brine percolation [10].

Textural equilibrium provides a powerful model to understand the first-order properties of complex polycrystalline two-phase materials based only on knowledge of the surface energies or, equivalently, the dihedral angle. Although Fig. 1 illustrates qualitative similarity between the model and observations, there is considerable debate if real systems approach equilibrium sufficiently for the model to be predictive. Computations of texturally equilibrated pores at isolated tetrahedral grain corners show accumulation of the melt along grain edges [Fig. 1(a)] and no wetting of entire grain boundaries [2,14–16]. If this theoretical prediction is true it places important bounds on various physical properties [25–27], which are generally hard to determine experimentally.

On the other hand, it is generally accepted that the observation of wetted grain boundaries would provide strong evidence that textural equilibrium has not been attained. Proving the existence of wetted grain boundaries conclusively, however, has been challenging. Initial attempts were not conclusive due to the limitations of manual serial sectioning and the difficulty of reconstructing three-dimensional geometries from two-dimensional images [28–31]. Later, microtomography provided three-dimensional images of the melt distribution [Fig. 1(a)], but the resolution of the images is not sufficient to conclusively image melt films along grain boundaries at low porosities [8]. Most recently, advances in high-resolution serial sectioning have provided evidence for wetted grain boundaries [32].

Here, we address the fundamental assumption underlying this debate and investigate if grain boundary wetting is possible in low-porosity texturally equilibrated networks. To resolve this question, we compute 3D texturally equilibrated pore networks for regular polycrystalline solids using a novel level set method. Surfaces of constant mean curvature are given by the steady-state solutions to interface motion driven by surface diffusion [33,34]. In a polycrystalline material with N grains, the surface of the ith grain is represented by the zero level set of a function φ_i. To compute the constant mean curvature solid-liquid interface we allow the surface of each grain to evolve by surface diffusion

$$(\varphi_i)_t + (\kappa_i)_{ss}|\nabla\varphi_i| = 0 \qquad \text{for } i = 1\ldots N, \tag{1}$$

where κ_{ss} is the surface Laplacian of the curvature, given by

$$\kappa_{ss} = [\nabla - \vec{n}(\vec{n}\cdot\nabla)][\nabla\kappa - \vec{n}(\vec{n}\cdot\nabla\kappa)], \tag{2}$$

where $\vec{n}$ is the outward normal and κ is the mean curvature. A surface diffusion rather than a mean curvature based evolution was chosen because it removes the gradients in curvature faster and handles changes in the sign of the curvature better. It also allows an effective implementation of the dihedral angle constraint. At the intersection of the ith and jth level sets mechanical equilibrium requires that

$$\vec{n}_i \cdot \vec{n}_j = \cos(\pi - \theta), \tag{3}$$

which can be enforced in the level set method [35]. This leads to a system of N nonlinear partial differential equations coupled through the dihedral angle constraints and a global constraint on the porosity of the medium. The initial condition for each level set (φ_i) is the implicit representation of the corresponding grain which can have any arbitrary shape. The texturally equilibrated pore network with dihedral angle θ and porosity ϕ is then given by the steady-state solution of this system. To obtain the numerical solution, κ_{ss} has been approximated with forth-order central differences, while convective and normal terms are discretized using the fifth-order Hamilton-Jacobi weighted essentially nonoscillatory scheme [36].

We compute texturally equilibrated pore networks in a regular polycrystalline solid comprised of truncated octahedra [Fig. 1(a)]. Figure 2 shows computed pore networks around a single grain for a range of dihedral angles and porosities. These confirm that the liquid is connected via channels along grain edges and forms a percolating pore network for all investigated ϕ when $\theta < 60°$. For $\theta > 60°$, the liquid shrinks along grain edges and forms isolated pores on corners where four grains meet. The percolation threshold for these isolated pores increases with the dihedral angle [14]. The grain edge channels that form above the percolation threshold are increasingly unstable due to a Rayleigh instability as θ increases [37].

In contrast to prevailing assumptions, the smaller square grain boundaries become fully wetted at $\theta = 10°$ and $\phi \geq 5\%$. Once the grain boundaries are wetted, the liquid resides in planar features on the grain boundaries and channels along grain edges have disappeared. In irregular natural materials with a larger distribution in the area of the grain boundaries this topological change is likely to be more gradual as the wetting proceeds from the smaller to the larger faces.

Ductile deformation of polycrystalline materials often generates a fabric of elongated and aligned grains that induces anisotropy in the physical properties of the porous medium. Strong anisotropic fabrics occur even in rock salt despite the cubic symmetry of the individual salt grains [24]. To explore the effect of anisotropic grain fabric on texturally equilibrated pore networks, we consider geometries where the solid grains have been stretched in the z direction by a factor f. The grains are oriented such that the stretching is normal to one of the square faces.

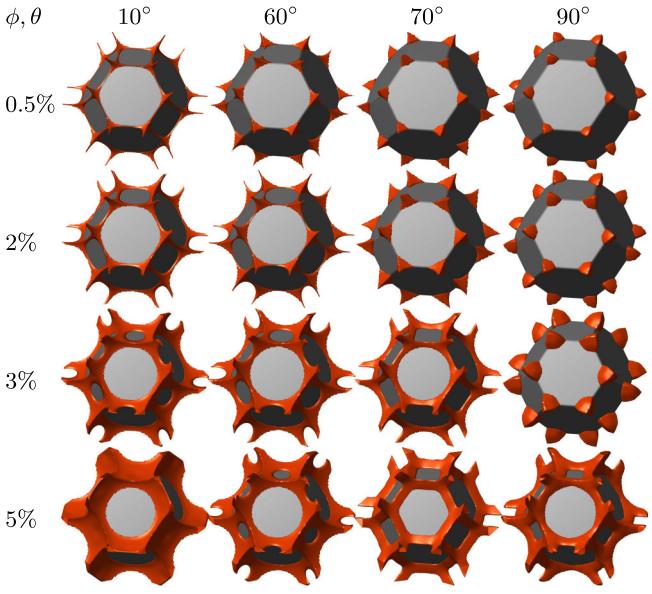

FIG. 2 (color online). Texturally equilibrated pore networks in a polycrystalline solid with an isotropic fabric. Only a single grain extracted from a network of 200 grains is shown.

Figure 3 illustrates that θ controls the geometry of the pore network that develops in a material with an anisotropic fabric. For $\theta < 60°$ the pores percolate for all ϕ investigated and the grain boundaries parallel to the direction of stretching are wetted once ϕ exceeds a threshold. Unlike isotropic media, where grain boundaries are only wetted at small θ, anisotropic fabrics also allow the wetting of grain boundaries at $\theta > 60°$. In this case, grain boundary wetting occurs at $\phi \approx 1.5\%$ for all $\theta > 60°$. The wetted boundaries are perpendicular to the stretching of the fabric but the pores do not percolate for the investigated range of ϕ. In anisotropic fabrics, grain boundary wetting is minimized

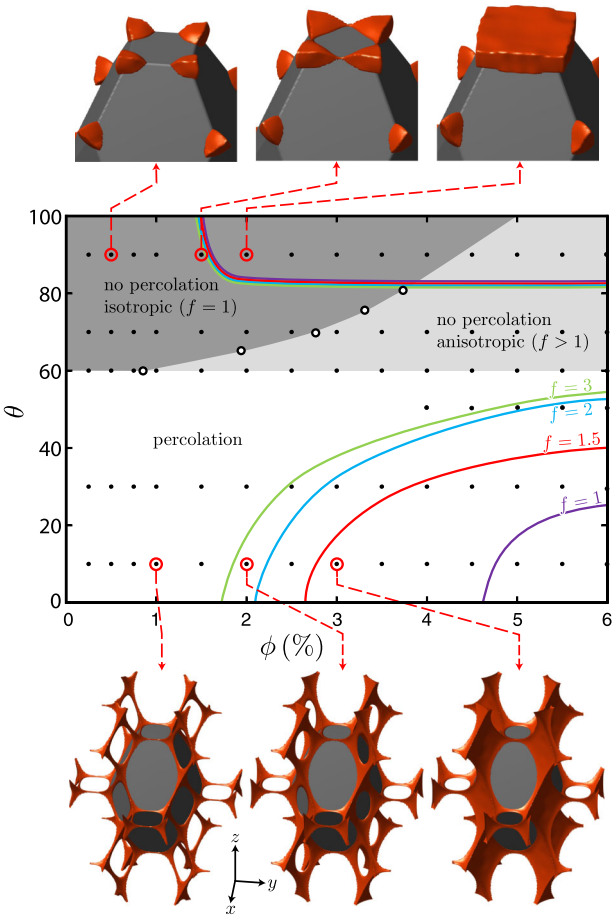

FIG. 3 (color online). The center shows a regime diagram for percolation and grain boundary wetting in $\phi\theta$ space. Black dots indicate the parameter combinations that have been investigated in this study. The dark gray region corresponds to conditions where isotropic media do not percolate. The black circles indicate the previously determined percolation boundary [14]. The expanded no percolation region for anisotropic media is shown in light gray. The colored contours indicate the boundaries where grain boundary wetting occurs for different anisotropies. The top row illustrates the formation of wetted grain boundaries for $\theta = 90°$ and $f = 1.5$ as ϕ increases from 0.5% to 2%. The bottom row illustrates the formation of wetted grain boundaries for $\theta = 10°$ and $f = 1.5$ as ϕ increases from 1% to 3%.

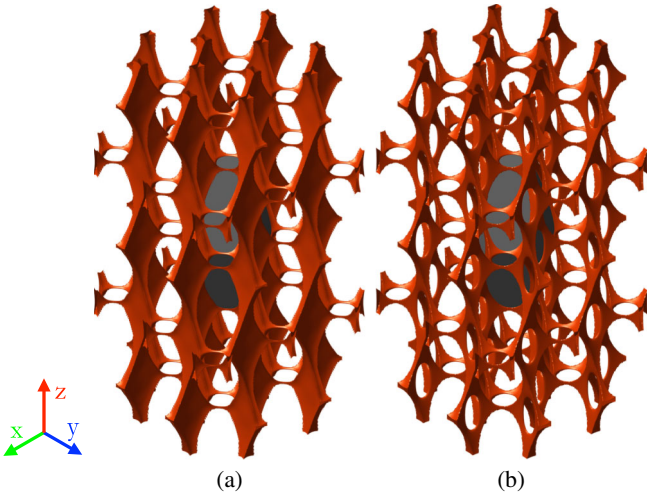

FIG. 4 (color online). Fluid distribution between grains in textural equilibrium with $f = 2$, porosity 3%. (a) $\theta = 10°$, (b) 60°. The polycrystalline material is stretched in the z direction.

for $\theta \approx 60°$. The percolation of the pore network and the occurrence of wetted grain boundaries is summarized in the regime diagram shown in Fig. 3. For $\theta < 60°$ grain boundary wetting occurs at smaller ϕ as the anisotropy of the fabric increases. Given the common occurrence of anisotropic fabrics in natural systems, wetting of the smaller grain boundaries should be common in texturally equilibrated pore networks.

Even very small stretching factors effectively prevent percolation of pores in materials with $\theta > 60°$, due to contraction of isolated pores illustrated in the top row of Fig. 3. In the isotropic fabric, shown in Fig. 2, all edges have the same length and the isolated pores connect simultaneously along all edges, once the percolation threshold is overcome. In the anisotropic fabric the pores first connect along the shortest edge. This change in the topology leads to a contraction of the pores along the other edges, so that subsequent percolation requires very large ϕ. Given the observed small ϕ of texturally equilibrated media, percolation at $\theta > 60°$ in solids with anisotropic fabric is unlikely. The basic connect-contract mechanism is the same in disordered media with variable grain size so that the percolation behavior will be similar.

In contrast to the isotropic case, both channels and tabular pores coexist in anisotropic pore networks at small θ. Since most of the liquid resides in the tabular pores parallel to the direction of stretching, the channels perpendicular to the stretching are very thin at small ϕ [Fig. 4(a)]. This suggests that strong anisotropies may exist in the physical properties of these pore networks. To test this hypothesis, the permeability of the texturally equilibrated pore networks has been calculated using lattice Boltzmann simulations [38]. Representative pore networks used in the computations are shown in Fig. 4. Both the vertical permeability, k_z, and the horizontal permeability, k_x, have been determined. Figure 5 only reports results for $\theta \leq 60°$ due to the lack of percolation at larger θ in anisotropic media.

Our simulations confirm that small amounts of anisotropy in the fabric of the porous media, $f \leq 3$, can induce dramatic permeability anisotropy, k_z/k_x. This anisotropy increases with f and is largest for small θ where the anisotropy in the fabric is amplified by 2 orders of magnitude [Figs. 5(b)–5(c)]. Although both k_x and k_z increase monotonically with ϕ, the permeability anisotropy reaches a pronounced maximum near $\phi = 2\%$ for $\theta < 60°$. This behavior can be understood in terms of the changes in the geometry of the pore network shown in the bottom row of Fig. 3. At low ϕ the connectivity in both directions is limited and the moderate permeability anisotropy is due to different lengths of the channels along the grain edges.

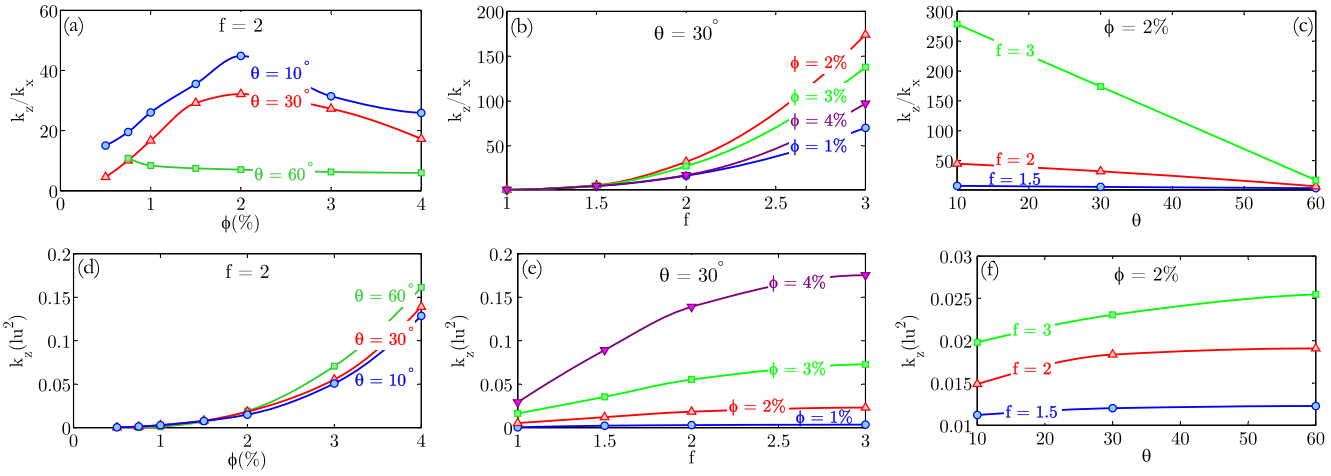

FIG. 5 (color online). (a-c) Development of permeability anisotropy in texturally equilibrated pore networks as function of ϕ, θ, and f. (d-e) Absolute permeability in texturally equilibrated pore networks as function of ϕ, θ, and f. In all cases, the polycrystalline material is stretched in the z direction.

As ϕ increases, the liquid begins to wet the grain boundaries parallel to the direction of stretching. The accumulation of liquid on the grain boundaries drains the channels providing horizontal connectivity and the permeability anisotropy reaches a maximum. A further increase in ϕ will increase the diameter of the channels and increase horizontal permeability, which leads to a decrease in k_z/k_x at larger ϕ. For $\theta \leq 60°$, the absolute permeability in the z direction increases with ϕ, f, and θ.

The results presented here demonstrate the complexity and richness of texturally equilibrated pore networks. In particular, we have demonstrated the existence of wetted grain boundaries at low porosities and finite dihedral angles as well as the dramatic effect the geometry of the pore network has on the physical properties of the medium, such as the permeability. This first exploratory study has focused on a simple ordered polycrystalline material, but the numerical approach is also applicable to disordered media. Grain boundary wetting is likely to be more common in disordered media and, therefore, also the induced permeability anisotropy and the increased percolation threshold for $\theta > 60°$ in anisotropic systems. The method can also be extended to include additional physics such as anisotropy in the surface energies. This will enable the exploration of a large variety of different phenomena and will complement tomographic studies of texturally equilibrated materials.

S. G. is supported by the Statoil Fellows Program at The University of Texas at Austin. M. H. was partially supported by NSF Grant No. EAR CMG-1025321.

*mhesse@ices.utexas.edu

[1] C. S. Smith, Trans. AIME **175**, 15 (1948).
[2] W. Beere, Acta Metall. **23**, 131 (1975).
[3] U. S. Schwarz and G. Gompper, Phys. Rev. Lett. **85**, 1472 (2000).
[4] B. A. DiDonna and R. D. Kamien, Phys. Rev. Lett. **89**, 215504 (2002).
[5] M. Tucker, J. Nucl. Mater. **79**, 199 (1979).
[6] J. W. Gibbs, *The Collected Works of J. Willard Gibbs* (Yale University Press, New Haven, CT, 1957).
[7] J. R. Bulau, H. S. Waff, and J. A. Tyburczy, J. Geophys. Res. **84**, 6102 (1979).
[8] W. Zhu, G. A. Gaetani, F. Fusseis, L. G. J. Montesi, and F. D. Carlo, Science **332**, 88 (2011).
[9] A. W. Rempel, E. D. Waddington, J. S. Wettlaufer, and M. G. Worster, Nature (London) **411**, 568 (2001).
[10] S. Lewis and M. Holness, Geology **24**, 431 (1996).
[11] D. Clarke, in *Surfaces and Interfaces of Ceramic Materials*, NATO ASI Series, Vol. 173, edited by L.-C. Dufour, C. Monty, and G. Petot-Ervas (Springer, Netherlands, 1989), p. 57.
[12] R. M. German, P. Suri, and S. J. Park, J. Mater. Sci. **44**, 1 (2009).
[13] M. Spiegelman and T. Elliott, Earth Planet. Sci. Lett. **118**, 1 (1993).
[14] N. von Bargen and H. S. Waff, J. Geophys. Res. **91**, 9261 (1986).
[15] M. J. Cheadle, Ph.D. thesis, University of Cambridge, 1989.
[16] J. F. Nye, J. Glaciol. **35**, 17 (1989).
[17] H. M. Mader, J. Glaciol. **38**, 333 (1992).
[18] E. W. Wolff and J. G. Paren, J. Geophys. Res. **89**, 9433 (1984).
[19] J. G. Dash, H. Fu, and J. S. Wettlaufer, Rep. Prog. Phys. **58**, 115 (1995).
[20] P. B. Price, Proc. Natl. Acad. Sci. U.S.A. **97**, 1247 (2000).
[21] H. M. Mader, M. E. Pettitt, J. L. Wadham, E. W. Wolff, and R. J. Parkes, Geology **34**, 169 (2006).
[22] M. W. Downey, AAPG bulletin **68**, 1752 (1984).
[23] M. B. Holness and S. Lewis, Geochim. Cosmochim. Acta **61**, 795 (1997).
[24] J. Schoenherr, J. L. Urai, P. A. Kukla, R. Littke, Z. Schlder, J.-M. Larroque, M. J. Newall, N. Al-Abry, H. A. Al-Siyabi, and Z. Rawahi, AAPG bulletin **91**, 1541 (2007).
[25] G. Hirth and D. L. Kohlstedt, J. Geophys. Res. **100**, 1981 (1995).
[26] Y. Takei, J. Geophys. Res. **107**, ECV6-1 (2002).
[27] A. L. Endres, T. Murray, A. D. Booth, and L. J. West, Geophys. Res. Lett. **36**, L04501 (2009).
[28] H. S. Waff and U. H. Faul, J. Geophys. Res. **97**, 9003 (1992).
[29] U. H. Faul, D. R. Toomey, and H. S. Waff, Geophys. Res. Lett. **21**, 29 (1994).
[30] U. H. Faul, J. Geophys. Res. **102**, 10299 (1997).
[31] M. Cmiral, J. D. F. Gerald, U. H. Faul, and D. H. Green, Contrib. Mineral. Petrol. **130**, 336 (1998).
[32] G. Garapić, U. H. Faul, and E. Brisson, Geochem. Geophys. Geosyst. **14**, 556 (2013).
[33] D. L. Chopp and J. A. Sethian, Interface. Free Bound. **1**, 107 (1999).
[34] P. Smereka, SIAM J. Sci. Comput. **19**, 439 (2003).
[35] E. Jettestuen, J. O. Helland, and M. Prodanović, Water Resour. Res. **49**, 4645 (2013).
[36] S. J. Osher and R. P. Fedkiw, *Level Set Methods and Dynamic Implicit Surfaces* (Springer, New York, 2002).
[37] W. Carter and A. Glaeser, Acta Metall. **35**, 237 (1987).
[38] C. Huber, A. Parmigiani, J. Latt, and J. Dufek, Water Resour. Res. **49**, 6371 (2013).